Journal of Power Sources 270 (2014) 121–130

Contents lists available at ScienceDirect

Journal of Power Sources

journal homepage: www.elsevier.com/locate/jpowsour

Synthesis, characterization and electrochemical performance of high-density aluminum substituted α-nickel hydroxide cathode material for nickel-based rechargeable batteries

Jing Li [a], Enbo Shangguan [a, *], Dan Guo [a], Meng Tian [a], Yanbin Wang [a], Quanmin Li [a], Zhaorong Chang [a, *], Xiao-Zi Yuan [b], Haijiang Wang [b]

[a] Collaborative Innovation Center of Henan Province for Green Manufacturing of Fine Chemicals, School of Chemistry and Chemical Engineering, Henan Normal University, Xinxiang 453007, PR China
[b] National Research Council of Canada, Vancouver, BC V6T 1W5, Canada

HIGHLIGHTS

- High-density Al-substituted α-$Ni(OH)_2$ was successfully synthesized via a novel route.
- The Al-substituted α-$Ni(OH)_2$ shows highest volume capacity of 469.6 mAh cm^{-3} at 5 C.
- The Al-substituted α-$Ni(OH)_2$ exhibits superior electrochemical cycle stability.

ARTICLE INFO

Article history:
Received 24 April 2014
Received in revised form
13 July 2014
Accepted 15 July 2014
Available online 23 July 2014

Keywords:
α-Nickel hydroxide
High tap-density
Nickel-based rechargeable batteries
Cathode materials

ABSTRACT

Positive electrode active materials, Al-substituted α-$Ni(OH)_2$, with a high tap-density and high performance for alkaline nickel-based rechargeable batteries have successfully been synthesized using a polyacrylamide (PAM) assisted two-step drying method and subsequent hydrothermal treatment at 140 °C for 2 h. X-ray diffraction (XRD), infrared spectroscopy (IR), scanning electron microscopy (SEM), laser particle size analysis, tap-density measurement, cyclic voltammetry (CV), electrochemical impedance spectroscopy (EIS), and charge–discharge test are used to characterize the physical and electrochemical properties of the synthesized material. The tap-density of the resulting powders reaches 1.84 g cm^{-3}, which is significantly higher than that of α-$Ni(OH)_2$ powders obtained by the conventional co-precipitation (CCP) and hydrothermal (HT) methods. Compared with commercial spherical β-$Ni(OH)_2$, the resulting sample is electrochemically more active, providing discharge capacities of 315.0 and 255.2 mAh g^{-1}, and volume capacities of 579.6 and 469.6 mAh cm^{-3} at rates of 0.2 C and 5 C, respectively. It is also found that although the hydrothermal treatment has a slight negative effect on the tap-density, it can improve the crystallinity of α-$Ni(OH)_2$ and promote the anion exchange of NO_3^- by OH^-, resulting in a much better electrochemical performance.

1. Introduction

As a result of excellent electrochemical properties, nickel hydroxide ($Ni(OH)_2$) has been intensively studied and widely used as a cathode material in all nickel-based alkaline secondary batteries, such as nickel–cadmium (Ni–Cd), nickel–metal hydride (Ni–MH), nickel–zinc (Ni–Zn) and nickel–ferrite (Ni–Fe) batteries [1–5]. There exist two nickel hydroxide polymorphs: α-$Ni(OH)_2$ and β-$Ni(OH)_2$, which can be transformed into γ-NiOOH and β-NiOOH, respectively, after the full electrochemical charging [6]. Owing to its high tap-density and excellent electrochemical performance, the spherical β-$Ni(OH)_2$ is widely used as cathode materials in commercial Ni-based alkaline secondary batteries. Corresponding to a single electron reaction in the β-$Ni(OH)_2$/β-NiOOH redox couple, the theoretical capacity of β-$Ni(OH)_2$ with a brucite-like structure is limited to 289 mAh g^{-1}. In contrast, α-$Ni(OH)_2$ with a turbostratic-disordered structure has a larger interlayer distance of about 8 Å, which is capable of realizing a two-electron reaction during the redox process between α-$Ni(OH)_2$/γ-NiOOH and is therefore

* Corresponding authors. Tel.: +86 373 3326335; fax: +86 373 3326336.
E-mail addresses: shangguanenbo@163.com (E. Shangguan), czr_56@163.com (Z. Chang).

http://dx.doi.org/10.1016/j.jpowsour.2014.07.098
0378-7753/

expected to have a much higher specific capacity [7]. Besides, as α-$Ni(OH)_2$ and γ-NiOOH are hydrated, α-$Ni(OH)_2$ can be cycled to γ-NiOOH reversibly without any mechanical deformation and constraints during cycling [7,8]. However, two main obstacles prevent the commercialization of α-$Ni(OH)_2$ [5,9,10]. One is that α-$Ni(OH)_2$ is unstable, and can easily be transformed to β-phase $Ni(OH)_2$ upon aging in a strong alkaline solution [9]. The other is the low tap-density (0.7–1.2 g cm^{-3}), which results in a low volumetric specific capacity.

Tremendous efforts have been made to improve the structural instability of the α-$Ni(OH)_2$ cathode material [11–28], for example, the so-called nickel aluminum layered double hydroxide (Ni–Al LDH). It has been found that the stability of α-$Ni(OH)_2$ can be achieved by partially substituting Al [11–16], Co [17–19], Fe [20,21], Mn [22–24], or Zn [25–28] ions for up to 20% of Ni ions. According to these studies, aluminum is considered the most effective element to enlarge the interlayer distance to form stabilized α-$Ni(OH)_2$ due to its high stability of the trivalent state and cheapness. Yet, the Al substitution approach has two side effects. One is that the discharge capacity usually decreases with increasing the amount of substituted Al because of the inefficiency of Al in the electrochemical redox reaction. The other is that tap-density greatly declines with the increase in the Al amount. This is mainly because that Al element has a much lighter atomic weight than Ni element regardless of the difference in the ionic radius between Ni^{2+} (0.69 Å) and Al^{3+} (0.54 Å) [29]. Also, to obtain a large enough size and high enough density of the particles co-precipitation of metals containing Al is very difficult [30]. For example, Chen [29] recently reported a complexation–coprecipitation method to prepare spherical Al-substituted α-$Ni(OH)_2$ samples for alkaline rechargeable batteries. The highest tap-density prepared by this method is only 1.1 g cm^{-3}, which is much lower than that of spherical β-$Ni(OH)_2$.

Considerable effort has been devoted to improving the electrochemical properties of Ni–Al LDH, including cationic substitution [31], additives [32,33], surface modification [34–37] and nanosized materials [38]. It is well established that crystallinity or morphology of the active materials has an important impact on their electrochemical properties [33–36]. Extensive researches have been conducted on the electrochemical performance of Al-substituted α-$Ni(OH)_2$ prepared by a hydrothermal method [39]. This method provides better crystallinity and higher discharge capacity of the material [39]. However, the preparation procedures are complex and the obtained $Ni(OH)_2$ can hardly meet the requirements for industrial mass production. Especially, the particles obtained by the hydrothermal method always exhibit a lower tap density (0.6–1.0 g cm^{-3}), which will result in a low volumetric specific capacity. A simple and economical method for synthesizing high-performance α-$Ni(OH)_2$ with high volumetric energy density is, therefore, craved, although it is quite challenging.

Up to now, reported literature on the enhancement in the tap-density of α-$Ni(OH)_2$ is scarce, despite the fact that tap-density makes the most significant difference for increasing the specific energy-density. In our previous studies we succeeded in synthesizing high-density non-spherical β-$Ni(OH)_2$ as a cathode material for Ni–MH batteries using a simple polyacrylamide (PAM) assisted two-step drying (PTSD) method [40,41]. The procedures are much simpler than those for spherical powders, more economical because there is no hydroxide-forming step, and more environmentally friendly as no ammonium is involved. On the basis of the above researches, we have come to strategy by combining the advantages of PTSD and HT methods to synthesize high performance α-$Ni(OH)_2$.

In the present study, high-density Al-substituted α-$Ni(OH)_2$ for alkaline secondary nickel-based battery cathode material was synthesized using a PTSD method with a subsequent hydrothermal treatment process at 140 °C for 2 h. The physical properties of the prepared nickel hydroxide were characterized by XRD, IR, SEM, TG-DTA, laser particle size analysis, and tap-density measurement, and the electrochemical properties were evaluated by CV, EIS, and charge–discharge test. For comparison, samples obtained by the conventional co-precipitation and the hydrothermal methods were also included in the test. It has been discovered that this new method not only dramatically increases the tap-density of the material, but also greatly improves its electrochemical performance.

2. Experimental

2.1. Synthesis of Al-substituted α-$Ni(OH)_2$

All of the reagents used in this work are of analytical grade without further purification. The Al-substituted α-$Ni(OH)_2$ samples obtained are denoted as follows—sample A: polyacrylamide (PAM) assisted two-step drying and hydrothermal treatment (PTSD + HT) method; sample B: PTSD method; sample C: the conventional co-precipitation (CCP) method;, and sample D: hydrothermal (HT) method.

Based on our previous report on the PTSD method [40,41], synthesis of sample A using the PTSD + HT method was diagramed in Fig. 1. A mixture of solution containing 2 M $Ni(NO_3)_2 \cdot 6H_2O$ and $Al(NO_3)_3 \cdot 9H_2O$ (in a [Ni^{2+}/Al^{3+}] ratio of 4:1) was added dropwise to 4 mol L^{-1} NaOH solution with constant stirring at 60 °C. After the reaction ceased, the resulting suspension was aged for 24 h in the mother solution at the same temperature, and then coagulated by adding PAM (25 mL PAM (0.6%) per 200 mL solution), filtrated

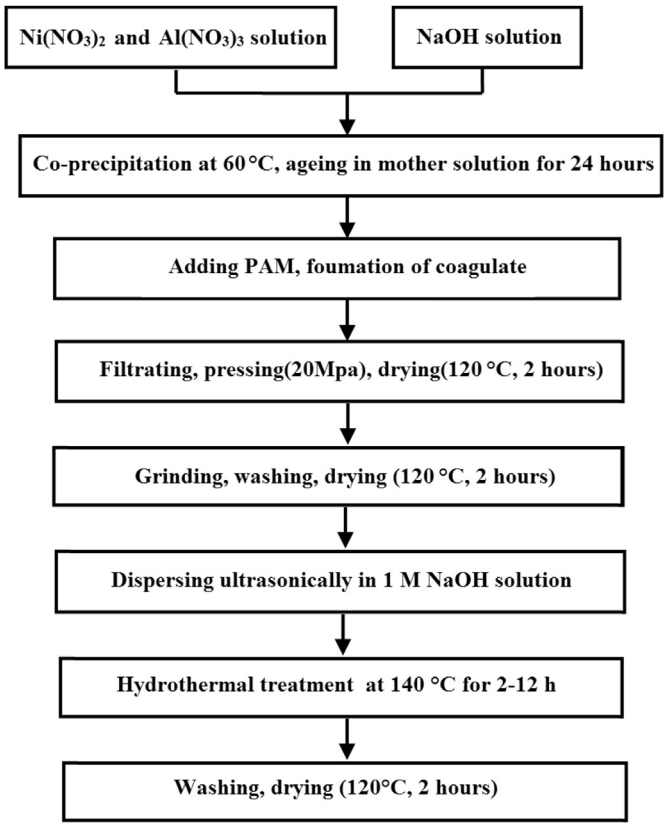

Fig. 1. Schematic diagram for the preparation of Al-substituted α-$Ni(OH)_2$ samples via the novel synthetic route.

(under a pressure of 20 MPa), dried (at 120 °C for 2 h), ground, washed, and dried (at 120 °C for 2 h) to obtain a green intermediate product. Then, 8 g of the precipitate formed at room temperature was ultrasonically redispersed in 70 mL 1 M NaOH solution. The suspension was then transferred to a Teflon-lined stainless steel autoclave with an inner volume of 100 mL. The autoclave was kept at 140 °C for 2–12 h, and then, naturally cooled to room temperature. After filtration, washing with distilled water, and drying at 120 °C for 2 h, the final product was obtained.

Sample B was synthesized by the PTSD method without hydrothermal treatment. The starting materials and proportions were the same as used in the PTSD + HT method.

Synthesis of sample C using the CCP method was carried out as follows: a mixture of solution containing 2 M $Ni(NO_3)_2 \cdot 6H_2O$ and $Al(NO_3)_3 \cdot 9H_2O$ (in a $[Ni^{2+}/Al^{3+}]$ ratio of 4:1) was added dropwise into a 4 M NaOH solution while stirring at 60 °C. After reaction, the precipitate was aged in the mother solution for 20 h at 50 °C and then washed with distilled water, filtered, and dried at 120 °C for 2 h.

Sample D was prepared using the HT method as follows: a mixture of solution containing 2 M $Ni(NO_3)_2 \cdot 6H_2O$ and $Al(NO_3)_3 \cdot 9H_2O$ (in a $[Ni^{2+}/Al^{3+}]$ ratio of 4:1) was added dropwise to 4 mol L^{-1} NaOH solution with constant stirring at 60 °C. After the reaction ceased, the suspension was then transferred to a Teflon-lined stainless steel autoclave. After sealing, the autoclave was kept at 140 °C for 20 h, and then naturally cooled to room temperature. The product was filtered, washed with distilled water, and dried at 120 °C for 2 h to produce Sample D.

2.2. Characterization of Al-substituted α-Ni(OH)$_2$

Phase analysis and cell parameter determination of all samples were performed by XRD using a D8 X diffractometer (Germany, Bruker) with Cu Kα radiation. The scan data were collected in a 2θ range of 5–80°. The step size was 0.026° with a counting time of 3 s. A SEM (SEM-6701F, JEOL, Japan) was used to examine the microstructures of the cathode material. IR spectra of the prepared samples were obtained on a Fourier infrared Bio-Rad FTS-40 spectrometer (KBr discs with a wave number of 400–4000 cm^{-1} and resolution of 0.09 cm^{-1}; and the measured sample weight of 2 mg). TG-DTA was carried out using an NETZSCH STA 409 PC/PG thermal analyzer (NETZSCH, Germany). Measurements were performed in air flow using α-Al_2O_3 as the reference material. The particle size distribution of the powders was obtained using an OMECLS-POP particle size analyzer (OMECLS, China). A JZ-1 tap-density tester (Chengdu Jingxin powder Analyzer Instruments Co., Ltd., China) was used to determine the tap-density of the samples. The metals content of the prepared samples was analyzed using inductively coupled plasma atomic emission spectroscopy (ICP-AES, IRIS Advantage). The elemental analysis of nitrogen was carried out with an element analyzer (EA, Perkin–Elmer 2400C).

2.3. Preparation of nickel electrode

Porous foamed nickel was cut into 2 cm × 2 cm squares as substrates. The pasted nickel electrodes were prepared as follows: 85 wt% Al-substituted α-$Ni(OH)_2$, 5.0 wt% CoO, and 5.0 wt% nickel powder were mixed thoroughly with a certain amount of 5 wt% PTFE solution to obtain a homogeneous slurry possessing adequate rheological properties. The slurry was poured into a foam nickel sheet and dried at 80 °C for 5 h. Subsequently, the pasted electrodes were pressed at 20 MPa for 3 min to assure good electrical contact between the foam nickel and the active material. For comparison, electrode were also similarly by adding 85 wt% of spherical β-$Ni(OH)_2$ into the nickel electrode as above. The used spherical β-$Ni(OH)_2$ was a commercial product (Henan Kelong Co., Ltd., China).

2.4. Electrochemical measurements

Electrochemical tests were performed in a three-compartment electrolysis cell at ambient temperature. Two nickel ribbon counter electrodes were placed in the side chambers and the working electrode was positioned in the center. The electrolyte was a solution of 6 M KOH + 15 g L^{-1} LiOH. A Hg/HgO reference electrode was used via a Luggin capillary, which was made in the same alkaline solution used in the working cell. CV and EIS were conducted on a Solartron SI 1260 impedance analyzer with a 1287 potentiostat interface. The CV test scan rate was between 1 mV s^{-1} and 10 mV s^{-1} and the cell potential ranged from 0.0 V to 0.7 V. For EIS, the impedance spectra were recorded at a 5 mV perturbation amplitude with a sweep frequency range of 10 kHz–1 mHz.

Test cells were assembled using the prepared nickel hydroxide electrode as the cathode, a hydrogen storage alloy electrode as the anode, and polypropylene to separate the cathode and anode. The electrolyte was a solution of 6 M KOH + 15 g L^{-1} LiOH. Charge/discharge measurements were conducted using a Land CT2001A battery performance testing instrument (Wuhan LAND Electronics Co., Ltd., China). For activation, twenty charge–discharge cycles at 0.2 C were performed, and the electrodes were discharged to 1.0 V. The batteries were then charged at a 0.2 C rate for 6 h and in sequence discharged at respective 0.2, 1, 2 C and 5 C discharge current rates under room temperatures. The cut-off voltages were set at 1.0 V, 1.0 V, 0.9 V, and 0.7 V, respectively. In the subsequent charge–discharge cycling tests, the batteries were charged at a 1 C rate for 72 min, rested for 20 min, and then discharged at 1 C discharge current rate (for sample A: 315 mA g^{-1}, sample B: 300 mA g^{-1}, sample C: 290 mA g^{-1}, sample D: 310 mA g^{-1}, spherical sample E: 260 mA g^{-1}). The cut-off voltages were set at 1.0 V. The discharge capacity of the nickel hydroxide in the positive electrode was based on the amount of active material (Al-substituted α-$Ni(OH)_2$) without taking into account the conducting additives in the electrode.

3. Results and discussion

3.1. Characterization of the as-synthesized samples

3.1.1. Physical properties

The chemical compositions and physical properties of Al-substituted α-$Ni(OH)_2$ samples A–D are presented in Table 1. As shown in Table 1, the tap-densities of samples A and B, prepared by the PTSD + HT method and the PTSD method, are 1.85 and 1.91 g cm^{-3}, respectively, remarkably higher than those of samples C obtained by the CCP method (1.36 g cm^{-3}) and D obtained by the HT method (0.82 g cm^{-3}). The mean diameters of samples A, B, C and D are 28.20, 27.53, 24.24 and 23.62 μm, respectively. The result clearly shows the significant effect of the synthetic method on tap-

Table 1
Physical properties of nickel hydroxide samples A, B, C and D.

Sample	Chemical composition			Ni^{2+}/Al^{3+} molar ratio	Tap-density (g cm^{-3})	Mean diameter (μm)
	Ni (wt%)	Al (wt%)	NO_3^- (wt%)			
A (PTSD + HT)	44.65	5.04	1.02	4.07	1.84	28.20
B (PTSD)	44.29	5.00	4.92	4.07	1.90	27.53
C (CCP)	43.96	4.96	4.05	4.08	1.36	24.24
D (HT)	44.72	5.05	4.29	4.07	0.82	23.62

density and the effectiveness of the PTSD method to improve the tap-density of Al-substituted α-Ni(OH)$_2$. As discussed in our previous work [39,40], addition of an appropriate amount of PAM into the Ni(OH)$_2$ suspension can result in agglomerations of colloid particles through the net structure formed, which can greatly accelerate filtration rate and reduce the moisture content in the press cake. Coagulation further increases the structure's density, as the agglomerations squeeze out water. Due to this dense structure, the Ni(OH)$_2$ particles are prone to grow and crystallize in the subsequent drying process, and the tap-density of the Ni(OH)$_2$ thereby remarkably increases.

It is notable that although hydrothermal treatment can result in better crystallinity, such hydrothermal treatment procedure has a greatly negative impact on the tap density of the synthesized sample. Fig. 2 shows the effects of hydrothermal treatment time on the tap density of nickel hydroxide powders. As the hydrothermal treatment time increases from 2 h to 12 h, the tap density declines from 1.91 to 0.83 g cm^{-3}, which may be attributable to the particle volume's expansion during the hydrothermal treatment process. To obtain high tap-density product, the optimum hydrothermal treatment time was 2 h.

Also in Table 1, it is found that although the molar ratio of Ni and Al are almost the same (about 4:1), the nickel and aluminum contents in samples A–D are slightly different. Interestingly, compared samples A with B, it can be found that after hydrothermal treatment, the NO_3^- content in sample A decreases from 4.92% to 1.02%. The result suggests that the use of alkaline solution provokes an anion exchange reaction between NO_3^- anions in the sample and OH^- anions in the solution during hydrothermal treatment process. As reported in a previous work [42], NO_3^- can be easily replaced by OH^- in alkaline solutions via the ion exchange reaction at room temperature and the exchange of NO_3^- by OH^- within the nickel hydroxide can significantly improve its electrochemical performances. So, it is expected that with hydrothermal treatment, sample A could possess some enhanced electrochemical performances, which are further proved by CV, EIS, and charge/discharge tests.

3.1.2. XRD

XRD patterns of the as-prepared Al-substituted α-Ni(OH)$_2$ samples A–D are presented in Fig. 3. Obviously, all the samples exhibit the same diffraction characteristics of Ni–Al LDH [2,38,43], iso-structural α-Ni(OH)$_2$·0.75H$_2$O (JCPDS card No. 38-0715). The asymmetrical diffraction peak located in the range of 32–36° is the characteristic of the turbostratic disorder in α-Ni(OH)$_2$ [44]. Also, peaks in the XRD patterns in Fig. 3 can be indexed to hexagonal

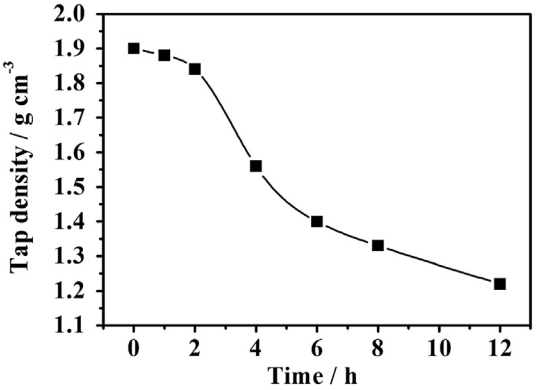

Fig. 2. The tap-density variation with the hydrothermal treatment time for Al-substituted α-Ni(OH)$_2$ samples.

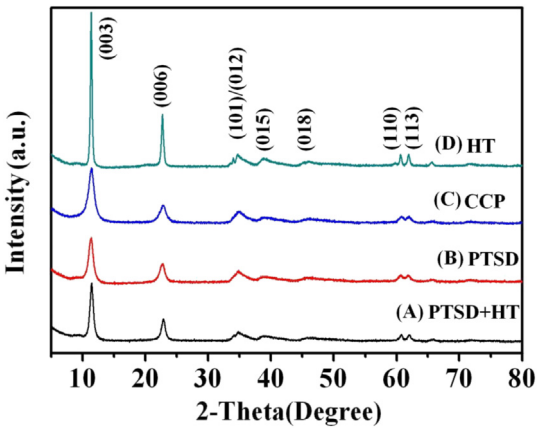

Fig. 3. XRD patterns of Al-substituted α-Ni(OH)$_2$ samples A, B, C, and D.

cells of space group *P*6222. It is noted that the diffraction intensity at (003) peak of sample A becomes stronger after hydrothermal treatment. An analysis of the XRD data in Fig. 3 is shown in Table 2, in which crystallite sizes are calculated based on the Scherrer equation using the strongest peak. It can be found that sample D has the biggest crystallite size and narrowest full width at half maximum (FWHM), which indicates the highest crystallinity of sample D. Also, it can be found that sample B without hydrothermal treatment has poorer crystallinity. After hydrothermal treatment, with the crystallite size increasing, sample A becomes more crystallized. This demonstrates that hydrothermal treatment facilitates the crystallinity of Al-substituted α-Ni(OH)$_2$ powders, even with a short time of 2 h.

3.1.3. IR spectra

The Fourier transform infrared (FTIR) spectra of the as-prepared Al-substituted α-Ni(OH)$_2$ samples A–D are shown in Fig. 4. All FTIR spectra show typical features of α-type nickel hydroxide [13,45]. The broad band at about 3480 cm^{-1} is characteristic of the stretching vibration of hydroxyl groups hydrogen-bonded to H$_2$O, and the band at about 1630 cm^{-1} corresponds to the bending mode of water molecules [14,17], indicating that there are many water molecules within the samples. As is well known, these water molecules may play an important role in improving the rate-capacity performance of the nickel hydroxide electrodes by providing the passage for proton diffusion along the molecular chain between the layers. The low band at about 1380 cm^{-1} in all FTIR spectra can be assigned to interference from the vibration of NO_3^- ion [42]. Also, it is possible that CO_3^{2-}, which also presents a peak at about 1365 cm^{-1}, interferes the measurements, as it is always a problem in LDH studies [11,46]. At low wave numbers, the band at about 640 cm^{-1} in all FTIR spectra is associated with the bending vibration Ni–O–H [3,13].

Table 2
Results of XRD analysis of nickel hydroxide samples A, B, C and D.

Sample	(003) 2θ, (°)	(003) FWHM, (°)	*d*-Value, (nm)	Crystallite size[a], (nm)	Lattice parameter	
					a (Å)	*c* (Å)
A (PTSD + HT)	11.31	0.569	7.7654	12.0	3.0515	23.3940
B (PTSD)	11.33	0.715	7.7551	11.0	3.0357	23.3102
C (CCP)	11.38	0.758	7.7483	10.4	3.0448	23.1990
D (HT)	11.32	0.296	7.7891	26.7	3.0998	23.4229

[a] Crystallite sizes were calculated based on the Scherrer equation, $D = K\lambda/B\cos\theta$, where $K = 0.89$, D is the particle size, $\lambda = 0.15406$ nm, B is the FWHM, and θ is the Bragg angle of the reflection.

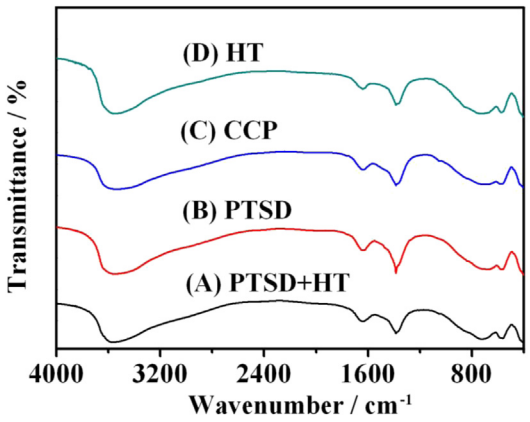

Fig. 4. IR spectra of Al-substituted α-Ni(OH)$_2$ samples A, B, C, and D.

3.1.4. TG–DTA

The amount of water molecules intercalated in nickel hydroxide plays an important role in the crystal structure and electrochemical properties. In this work, TG–DTA analyses were used to investigate the water content and dehydration reactions of the nickel hydroxide. The TG and DTA curves for samples A–D are shown in Fig. 5. All four samples show two weight loss regions. The first region is below 200 °C there in structurally bonded water is removed. The second region between 200 °C and 470 °C is due to Al-substituted α-Ni(OH)$_2$ being decomposed into Ni–Al LDO (layered double oxide), H_2O, and the loss of adsorbed and intercalated anions (nitrate ions and carbonate ions) [4,47]. The total water content of samples A, B, C and D are about 12.87 wt%, 14.39 wt%, 15.61 wt%, and 9.41 wt%, respectively. The result illustrates that the different synthetic methods have marked impact on the moisture content in the final product. As is seen, sample D has the lowest water content and the water content of sample A is a little lower than that of sample B, suggesting that the hydrothermal process can greatly reduce the moisture content. In addition, the use of the PTSD method can also reduce the moisture content, which is in accordance with our previous work [40]. It is well known that the structurally bonded water (intercalated water) molecules in nickel hydroxide can provide the passage for proton diffusion along the molecular chain between layers, which may accelerate the proton diffusion rate. As such, the samples with different moisture contents may show different electrochemical performances.

3.1.5. SEM

Fig. 6 displays SEM photographs of samples A–D. It can be seen that all samples appear to be aggregates of irregular shapes, very similar to the Al-substituted α-Ni(OH)$_2$ powders prepared by homogenous precipitation method [18]. The irregular shapes may result from grinding, which leads to a higher specific surface area and more structural disorder [40,41]. Generally, the nickel hydroxide powers with irregular tabular shapes have a higher specific surface area that can provide a high density of active sites and thereby promote intimate interaction between the active material and the surrounding electrolyte [40]. In addition, the particles of samples A and B obtained by the HTSD method seem more denser than the others. It is also seen that in comparison to sample A, sample B without hydrothermal treatments exhibits larger and more dense particles, indicating the significant impact of hydrothermal treatments on the particle morphology.

3.2. Electrochemical investigation of the as-synthesized samples

3.2.1. CV measurements of nickel electrode

Fig. 7 illustrates the typical CV curves for samples A–D at various scan rates and 25 °C. For all the electrodes, one anodic oxidation peak and one cathodic reduction peak are observable on the CV curves. The redox peaks can be assigned to the reversible electron transfer process of Ni(OH)$_2$ described by the following well-accepted reaction:

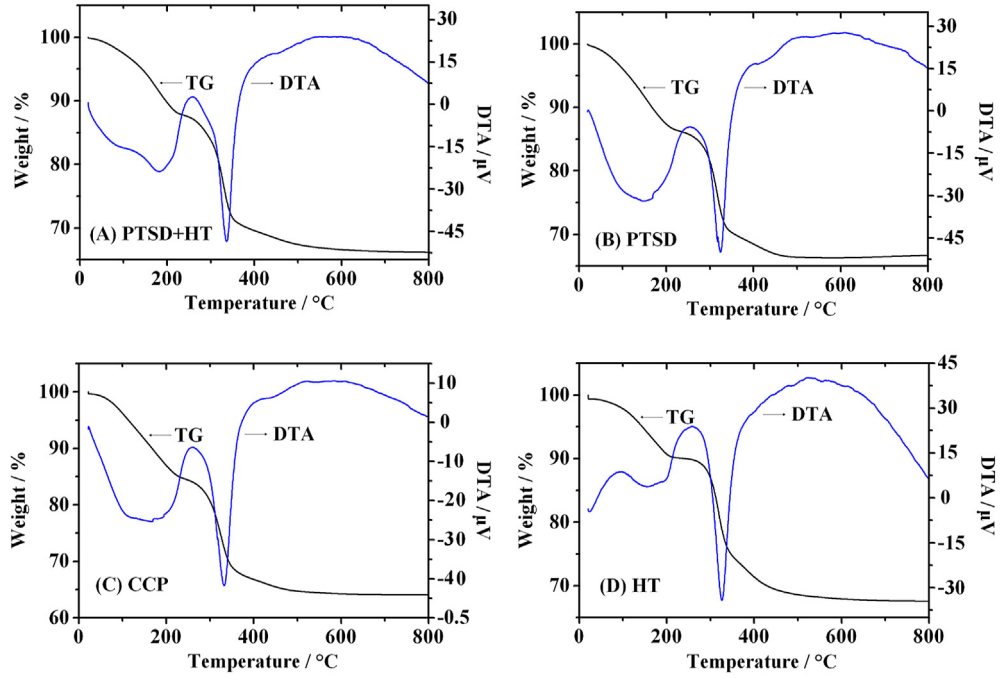

Fig. 5. TG and DTA plots for Al-substituted α-Ni(OH)$_2$ samples A, B, C, and D.

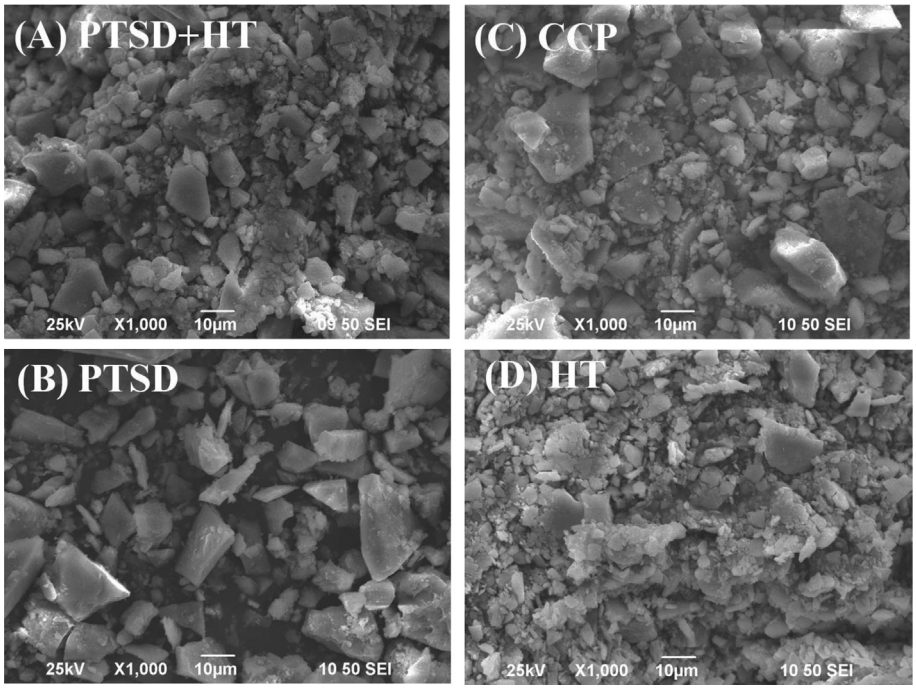

Fig. 6. SEM images of Al-substituted α-$Ni(OH)_2$ samples A, B, C, and D.

$$\alpha-[Ni_{1-x}Al_x(OH)_2]A_y+OH^- \rightleftarrows \gamma-[Ni_{1-x}Al_xOOH]A_y+H_2O+e^- \quad (1)$$

where A represents an anion such as NO_3^-, CO_3^{2-}, OH; and x, y are numbers. As the scan rate increases from 1 to 10 mV s^{-1}, the peak current increases. At different scan rates, all the redox peaks on CV curves can clearly be observed. Although the peak shapes are similar to each other, the peak potentials shift to the respective anodic and cathodic directions, due to the increased polarization at a high scan rate.

To compare the CV characteristics of all electrodes, the results of CV measurements at a scan rate of 1 mV s^{-1} are tabulated in Table 3. Generally, the potential difference ($\Delta(E_{O-R})$) between the oxidation (E_O) and reduction (E_R) potentials can be employed to characterize the reversibility of the redox reaction [36,41]. Smaller $\Delta(E_{O-R})$ suggests that the electrode reaction is more reversible. As shown in Table 3, the $\Delta(E_{O-R})$ apparently differs with the following trend: D (HT) (119 mV) < A (PTSD + HT) (131 mV) < B (PTSD) (142 mV) < C (CCP) (144 mV). This indicates that the charge and discharge process of sample A is more reversible than that of samples B and C. The result also proves that the hydrothermal treatment facilitates the redox reversibility.

Usually, the charge process of the $Ni(OH)_2$ electrode occurs in competition with a parasitic oxygen evolution reaction, which obscures the baseline of the oxidation peak current and limits the electrochemical performance of the $Ni(OH)_2$ electrodes. The difference between the oxygen evolution potential and the oxidation peak potential $\Delta(E_{oe-O})$ of the samples is, thus, an important parameter for judging the performance of electrode materials. The high $\Delta(E_{oe-O})$ value facilitates the electrode to be fully charged before oxygen evolution. The greater the $\Delta(E_{oe-O})$, the better the charge efficiency and acceptance. As shown in Table 3, the $\Delta(E_{oe-O})$ decreases in the following trend: A (PTSD + HT) (101 mV) > D (HT) (95 mV) > B (PTSD) (92 mV) > C (CCP) (85 mV). This means that sample A obtained by the new method exhibits a higher charge efficiency of the electrode and a high reutilization of the active material before oxygen evolution.

As is well known, the electrochemical reaction process of a nickel hydroxide electrode is limited by proton diffusion through the lattice [5,41]. The increase in the proton diffusion rate will decrease the electrode polarization during the charge–discharge process. The proton diffusion rate can be decided by the proton diffusion coefficient. It is, therefore, of great importance to study the nickel electrode's proton diffusion coefficient. Fig. 7(E) shows the plots of the anodic peak current (i_p) vs. the square root of the scan rate ($v^{1/2}$) obtained from Fig. 7(A)–(D). The proton diffusion coefficient of the $Ni(OH)_2$ electrode can be obtained from the slope of the plots. In the case of semi-infinite diffusion, the peak current, i_p, on the CV can be expressed by the Sevick equation at 25 °C [41,48]:

$$i_p = 2.69\times10^5\times n^{3/2}\times A\times D^{1/2}\times C_0\times v^{1/2} \quad (2)$$

where n is the number of the electrons transferred, A is the surface area of the electrode, D is the diffusion coefficient, v is the scanning rate, and C_0 is the proton concentration. For samples A–D, the n, A, C_0 and v can be considered the same. Based on the classical Eq. (2), the proton diffusion coefficient only depends on the slope of i_p vs. $v^{1/2}$ in Fig. 7(e). It is noteworthy that the slopes of i_p vs. $v^{1/2}$ in Fig. 7(e) are in the order of A (PTSD + HT) > D (HT) > B (PTSD) > C (CCP), resulting in a proton diffusion coefficient trend of A (PTSD + HT) > D (HT) > B (PTSD) > C (CCP). The increase in the proton diffusion favors the fast ionic transportation, accelerates the electrode reaction and decreases the electrode polarization during the charge–discharge process [48]. Evidently, sample A has the highest proton diffusion coefficient, indicating a fast electrode reaction due to the fast ionic transportation.

3.2.2. EIS measurements of nickel electrode

Fig. 8 presents the electrochemical impedance spectra for electrodes A–D at a steady state. Clearly, the Nyquist plot for each sample displays a depressed semicircle resulting from charge transfer resistance (R_{ct}) in the high-frequency region, and a slope related to Warburg impedance in the low-frequency region [41,48].

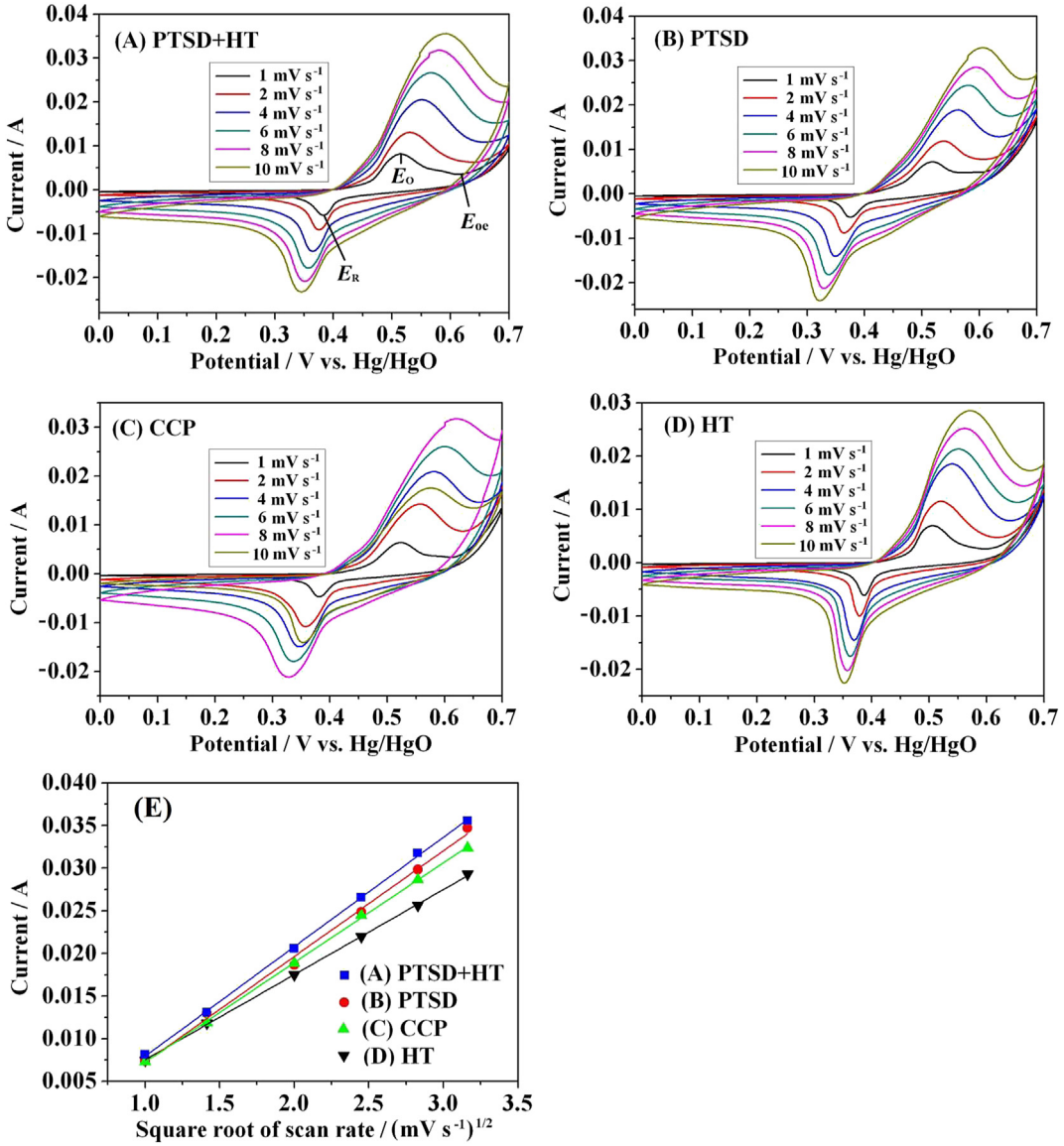

Fig. 7. Cyclic voltammograms of Al-substituted α-Ni(OH)$_2$ samples A (A), B (B), C (C), and D (D) at various scan rates. (E) Relationship between the cathodic peak current (i_p) and the square root of the scan rate for Al-substituted α-Ni(OH)$_2$ samples A, B, C, and D.

To obtain the charge-transfer resistance of the electrodes, an equivalent circuit is used to fit these experimental data as shown in Fig. 8, in which R_s represents the total resistance of the solution, CPE is the constant phase element related to the double layer capacitance, R_{ct} is the charge-transfer resistance of the electrode, and W is the generalized finite Warburg impedance of the solid phase diffusion. The simulated values of the elements based on the equivalent circuit are listed in Table 4, where it can be seen that the R_{ct} and W values of electrode A the lowest, which implies that the electrochemical reaction on electrode A proceeds more easily than on other electrodes.

The higher proton diffusion coefficient and lower charge transfer resistance in the as-prepared Al-substituted α-Ni(OH)$_2$

Table 3
Characteristic potential values from CV curves for samples A, B, C and D.

Electrode	E_O (mV)	E_R (mV)	E_{oe} (mV)	$\Delta(E_{O-R})$ (mV)	$\Delta(E_{oe-O})$ (mV)
A (PTSD + HT)	0.515	0.383	0.616	132	101
B (PTSD)	0.518	0.374	0.610	144	92
C (CCP)	0.524	0.381	0.609	143	85
D (HT)	0.506	0.387	0.601	119	95

Note: E_O and E_R is the oxidative and reductive potential; $\Delta(E_{O-R})$ is the difference between E_O and E_R; E_{oe} for oxygen revolution potential; $\Delta(E_{oe-O})$ is the difference of the oxidative and oxygen revolution potential.

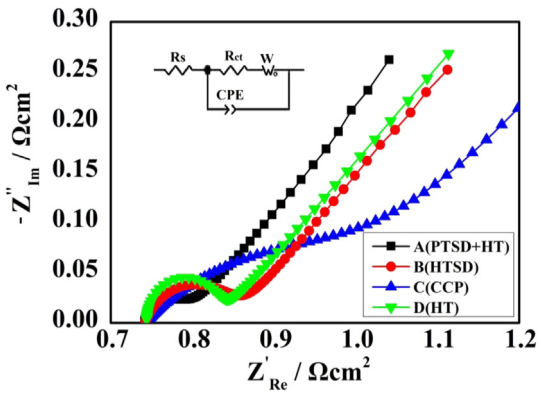

Fig. 8. Electrochemical impedance spectra of electrodes A, B, C, and D at 25 °C.

Table 4
Parameters from EIS measurements of nickel electrodes A, B, C and D.

Electrode	R_s (Ω cm^2)	CPE (F cm^{-2})	R_{ct} (Ω cm^2)	W (Ω cm^2)
A (PTSD + HT)	0.7425	0.05116	0.0565	6.950
B (PTSD)	0.7409	0.04835	0.1209	9.761
C (CCP)	0.7426	0.06348	0.3761	9.563
D (HT)	0.7438	0.04105	0.1187	8.121

sample A can be attributable to more compact structure, improved crystallinity and the introduction of OH^- anion into the interlayer space. Firstly, the different proton diffusion coefficients of the as-prepared Al-substituted α-$Ni(OH)_2$ samples may be related to the different proton/electron diffusion routes resulting from the different solid structures. In our previous work, we have found that the dense solid structure in high-density nickel hydroxide is beneficial for the acceleration of solid-state proton diffusion in the $Ni(OH)_2$ lattice. A more compact structure leads to a shorter proton diffusion route, which results in a higher proton diffusion coefficient. Secondly, it is well-known that crystallinity of the active materials has an important impact on the electrochemical properties [2,4]. Better crystallinity is conducive to higher discharge capacity and better cyclic performance. The better electrochemical activity of sample A is attributable to the improved material crystallinity resulted from the hydrothermal treatment. Thirdly, for Al-substituted α-$Ni(OH)_2$, it has been discovered that the interlayer anions may have great effects on the proton migration. OH^- anion can be introduced into the interlayer space by ion exchange to improve the ionic conductivity, which facilitates the rapid movement of proton in the $Ni(OH)_2$ lattice [42]. It is generally known that NO_3^- can easily be replaced by OH^-. In the present work, it has also been proved that the amount of intercalated NO_3^- anions in sample A greatly decrease after hydrothermal treatment in the alkaline solution (see Table 1). In brief, these facts account for the better performance of Al-substituted α-$Ni(OH)_2$ sample A.

3.3. Charge/discharge test of nickel electrodes

To evaluate the feasibility of the as-prepared Al-substituted α-$Ni(OH)_2$ as cathode materials for commercial nickel-based secondary batteries, this study also compares the electrochemical performance between the as-prepared samples and commercial spherical β-$Ni(OH)_2$. Fig. 9 shows the charge and discharge curves of nickel electrodes A–E electrodes at rates of 0.2, 1, 2, and 5 C,

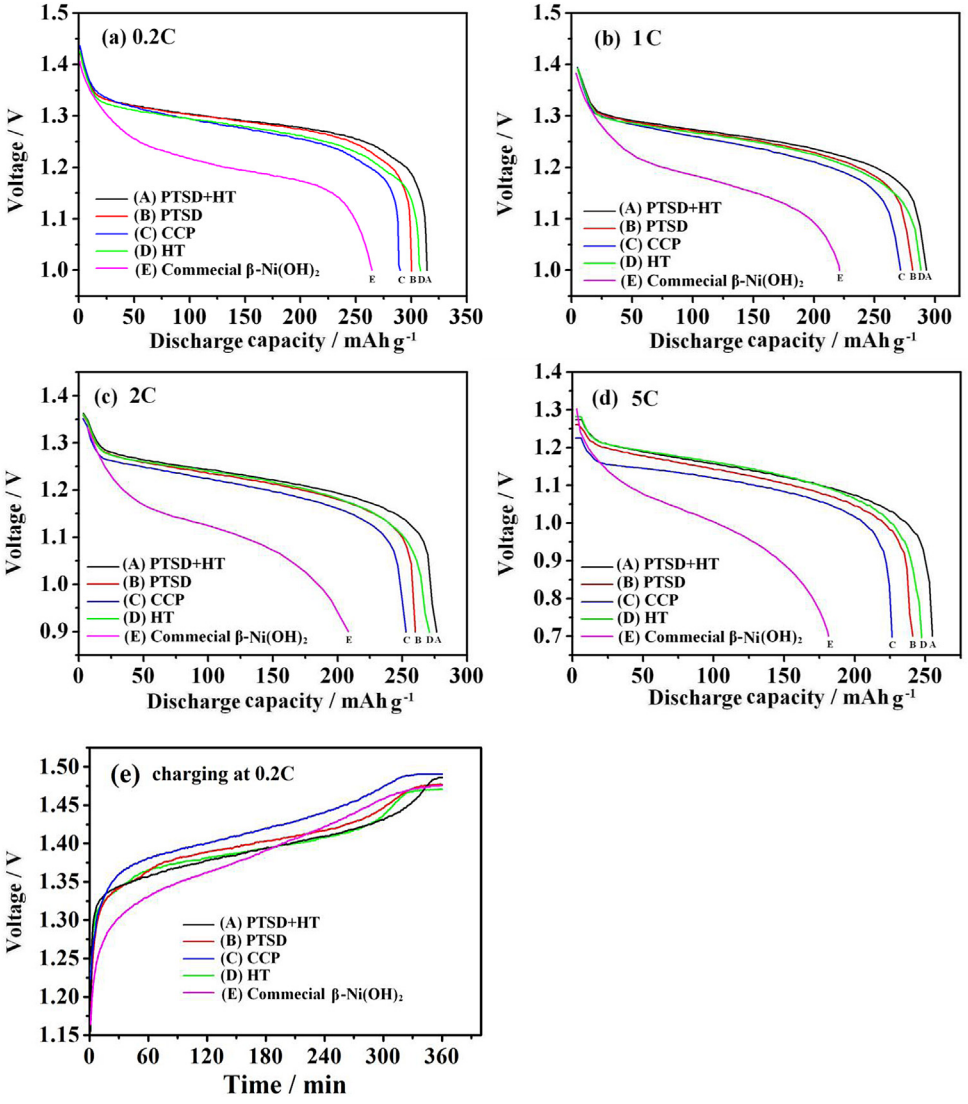

Fig. 9. Charge and discharge curves of the electrodes prepared with samples A, B, C, D, and E at different current rates.

Table 5
Results of the charge/discharge test for different electrodes at different current rates.

Electrode	Tap-density (g cm^{-3})	Specific capacity (mAh g^{-1})				Specific volume capacity (mAh cm^{-3})			
		0.2 C	1 C	2 C	5 C	0.2 C	1 C	2 C	5 C
A (PTSD + HT)	1.84	315.0	292.8	276.7	255.2	579.6	538.7	509.1	469.6
B (PTSD)	1.90	300.4	281.5	260.2	241.1	570.8	534.8	494.4	458.1
C (CCP)	1.36	291.5	271.6	252.9	226.5	396.4	369.4	343.9	308.0
D (HT)	0.82	310.5	288.4	270.9	247.6	254.6	236.5	222.1	203.0
Spherical	2.20	262.7	232.0	206.1	189.6	577.9	510.4	453.4	417.1

respectively, where sample E is the electrode made from commercial spherical β-Ni(OH)$_2$. The experimental results are given in Table 5. Obviously, the specific discharge capacities (especially for the volume capacity) of sample A are higher than those of samples B–D. For example, at a rate of 0.2 C, sample A shows a volume capacity of 579.6 mAh cm^{-3}, which is significantly higher than those of C (396.4 mAh cm^{-3}) and D (254.6 mAh cm^{-3}). Compared sample A with sample B, it can be found that although the tap density slightly decreases after hydrothermal treatment at 140 °C for 2 h, sample A still has a higher volume capacity, which mainly results from the enhanced electrochemical performance. In brief, sample A prepared by the new method exhibits not only a high tap density, but also excellent electrochemical performance, resulting in a higher volume capacity than commercial sample E.

It is also clear that all the Al-substituted α-Ni(OH)$_2$ samples exhibit a higher discharge capacity and higher discharge potential plateau than electrode E with commercial spherical β-Ni(OH)$_2$ at the same discharge rate (0.2 C, 1 C, 2 C and 5 C). However, the volume capacity of samples C and D obtained by the CCP and HT methods is greatly lower than that of commercial spherical sample E at all discharge rates, illustrating that the samples obtained by the CCP and HT methods do not meet the demand for commercial product.

As shown in Table 5, as the discharge rate increases from 0.2 to 5 C, the discharge capacity of sample A decreases from 315.0 to 255.2 mAh g^{-1}, showing that at such a high discharge rate 81.0% capacity is still retained. In contrast, the discharge capacity of commercial sample E decreases from 262.7 to 189.6 mAh g^{-1}, showing capacity retention of about 72.2%. Especially, at a 5 C rate, sample A shows a higher discharge capacity of 255.2 mAh g^{-1} and a volume capacity of 469.6 mAh cm^{-3}, whereas the values for sample E are only 189.6 mAh g^{-1} and 417.1 mAh cm^{-3}, respectively, indicating that the high-rate performance of sample A obtained by the new method is much better than that of the commercial spherical sample.

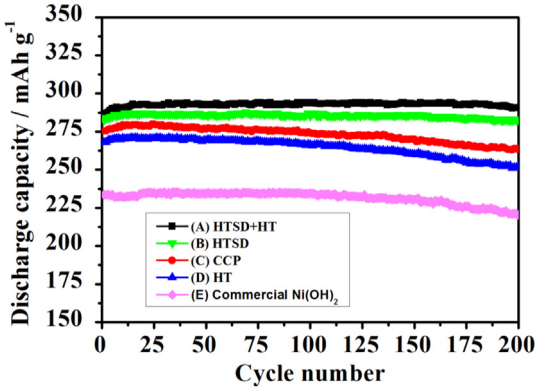

Fig. 10. Cyclic performance of the prepared electrodes A, B, C, D, and E at 1 C charge/discharge rate.

The cyclic performance of nickel electrodes A–E at a 1 C rate is illustrated in Fig. 10. Obviously, electrode A shows higher specific capacity and better cycling stability than other electrodes. To quantitatively characterize the cyclic stability of the nickel electrodes, the deterioration rate (R_d) is used, where R_d is equal to $(C_m - C_i)/C_m$ (C_m: maximum capacity; C_i: capacity at a certain cycle). The R_d at the 200th cycle for nickel electrodes A, B, C, D and E are 97.8%, 93.3%, 91.0%, 97.2% and 93.6%, respectively, which indicates that the Al-substituted α-Ni(OH)$_2$ powders prepared by the new method have much better cyclic stability and higher discharge capacity than the powder obtained by the other methods. Especially, a higher capacity (27.0% more than the corresponding spherical β-Ni(OH)$_2$) is observed for sample A in all cycles. Clearly, the overall electrochemical performance of Al-substituted α-nickel hydroxide prepared by the new method is superior to the commercial spherical Ni(OH)$_2$.

In summary, the Al-substituted α-nickel hydroxide prepared by the new method has demonstrated not only a high tap density, but also excellent electrochemical performance. This electrochemical performance improvement is attributable to the compact microstructure, improved crystallinity and the introduction of OH$^-$ anion into the interlayer space, thus resulting in a better reaction reversibility, higher proton diffusion coefficient, and lower electrochemical impedance of the material, as indicated by CV and EIS. The results also illustrate that hydrothermal treatment is a key factor to improve the electrochemical performance for Al-substituted α-nickel hydroxide, such as the discharge capacity, high-rate discharge ability, and cycle stability. In addition, owing to the substitution of 20% cheap Al for Ni element, the new method reduces the material cost by about 18%. Accordingly, the proposed PTSD + HT method is promising for electrochemical performance improvement and effective for cost reduction if used in alkaline rechargeable nickel-based batteries.

4. Conclusions

High density and high performance positive electrode active materials, Al-substituted α-Ni(OH)$_2$ powders, were successfully synthesized using a polyacrylamide (PAM) assisted two-step drying method and subsequent hydrothermal treatment at 140 °C for 2 h. The tap-density of the powders reaches 1.84 g cm^{-3}, which is notably higher than that of Ni(OH)$_2$ powders obtained by the CCP method and the HT method. The as-prepared α-Ni(OH)$_2$ samples obtained by the proposed method exhibit excellent electrochemical performance, compared with, samples prepared by other methods, with better reaction reversibility, higher proton diffusion coefficient, lower charge transfer resistance, higher specific capacity, and better cyclic stability. Especially, the specific volume capacity of sample A reaches 469.6 mAh cm^{-3} at 5 C, much higher than that of commercial spherical Ni(OH)$_2$. It is also found that although hydrothermal treatment has a significantly negative impact on the tap-density of the sample, hydrothermal treatment for a short time still plays a key role in improving the electrochemical performance of the powders. This performance improvement could be

attributable to the anion exchange of NO_3^- by OH^- and higher crystallinity, both resulting from the hydrothermal treatment process. The new method is also simple and facile for synthesizing Al-substituted α-$Ni(OH)_2$ powders with high tap-density and high performance. Due to the lower cost and outstanding performance, the sample synthesized by the proposed method is a promising positive electrode active material for alkaline nickel-based rechargeable batteries.

Acknowledgments

The authors thank the financial supports from the Joint Funds of the National Natural Science Foundation of China (No. U1304211), Henan Education Bureau Foundation of China (Nos. 13A150507 and 13A150512), Henan Provincial Department of Science and Technology Foundation of China (Nos. 132300410294 and 132300410299) and Henan Key Science and Technology Program of China (No. 132102210256).

References

[1] V. Ganesh Kumar, N. Munichandraiah, P. Vishnu Kamath, A.K. Shukla, J. Power Sources 56 (1995) 111–114.
[2] W.K. Hu, D. Noreus, Chem. Mater. 15 (2003) 974–978.
[3] T.N. Ramesh, P. Vishnu Kamath, J. Power Sources 156 (2006) 655–661.
[4] W.K. Hu, X.P. Gao, D. Noreus, T. Burchardt, N.K. Nakstad, J. Power Sources 160 (2006) 704–710.
[5] M.A. Kiani, M.F. Mousavi, S. Ghasemi, J. Power Sources 195 (2010) 5794–5800.
[6] Y. Sato, S. Takeuchi, K. Kobayakawa, J. Power Sources 93 (2001) 20–24.
[7] X.P. Gao, H.X. Yang, Energy Environ. Sci. 3 (2010) 174–189.
[8] A.K. Shukla, S. Venugopalan, B. Hariprakash, J. Power Sources 100 (2001) 125–148.
[9] A. DelahayeeVidal, B. Beaudoin, N. SaceEpée, K. TekaiaeElhsissen, A. Audemer, M. Figlarz, Solid State Ionics 84 (1996) 239–248.
[10] J.X. Dai, F.Y. Sam, T. Li, Danny Xiao, Donald M. Wang, E. David, S. Reisner, J. Power Sources 89 (2000) 40–45.
[11] K.T. Ehlsissen, A. DelahayeeVidal, P. Genin, M. Figlarz, P. Willmann, J. Mater. Chem. 3 (1993) 883–888.
[12] P.V. Kamath, M. Dixit, L. Indira, A.K. Shula, V.G. Kumar, N. Munichandraiah, J. Electrochem. Soc. 141 (1994) 2956–2959.
[13] Y.W. Li, J.H. Yao, C.J. Liu, W.M. Zhao, W.X. Deng, S.K. Zhong, Int. J. Hydrogen Energy 35 (2010) 2539–2545.
[14] Y.L. Zhao, J.M. Wang, H. Chen, T. Pan, J.Q. Zhang, C.N. Cao, Int. J. Hydrogen Energy 29 (2004) 889–896.
[15] L.J. Yang, X.P. Gao, Q.D. Wu, H.Y. Zhu, G.L. Pan, J. Phys. Chem. C 111 (2007) 4614–4619.
[16] C.Y. Wang, S. Zhong, K. Konstantinov, G. Walter, H.K. Liu, Solid State Ionics 148 (2002) 503–508.
[17] C. Faure, C. Delmas, P. willmann, J. Power Sources 36 (1991) 497–506.
[18] Y.L. Zhao, J.M. Wang, H. Chen, T. Pan, J.Q. Zhang, C.N. Cao, Electrochim. Acta 50 (2004) 91–98.
[19] B. Mavis, M. Akinc, J. Power Sources 134 (2004) 308–317.
[20] L. Demourguese-Guerlou, C. Delmas, J. Power Sources 45 (1993) 281–289.
[21] J. Qiu, G. Villemure, J. Electroanal. Chem. 428 (1997) 165–172.
[22] L. Indira, M. Dixit, P.V. Kamath, J. Power Sources 52 (1994) 93–97.
[23] R.S. Jayashree, P.V. Kamath, J. Power Sources 107 (2002) 120–124.
[24] M. Morishita, S. Ochiai, T. Kakeya, T. Ozaki, Y. Kawabe, M. Watada, S. Tanase, T. Sakai, J. Electrochem. Soc. 155 (2008) A936–A944.
[25] C. Tessier, L. GuerlouеDemourgues, C. Faure, A. Demourgues, C. Delmas, J. Mater. Chem. 10 (2000) 1185–1193.
[26] H. Chen, J.M. Wang, T. Pan, H.M. Xiao, J.Q. Zhang, C.N. Cao, Int. J. Hydrogen Energy 27 (2002) 489–496.
[27] M. Dixit, P.V. Kamath, J. Gopalakrishnan, J. Electrochem. Soc. 146 (1999) 79–82.
[28] X.R. Gao, L.X. Lei, M. Hu, L.W. Qin, Y.M. Sun, J. Power Sources 191 (2009) 662–668.
[29] H. Chen, J.M. Wang, T. Pan, Y.L. Zhao, J.Q. Zhang, C.N. Cao, J. Power Sources 143 (2005) 243–255.
[30] Yongseon Kim, Doyu Kim, ACS Appl. Mater. Interfaces 4 (2012) 586–589.
[31] Alexis Bienvenu Béléké, Minoru Mizuhata, J. Power Sources 195 (2010) 7669–7676.
[32] H. Chen, J.M. Wang, T. Pan, Y.L. Zhao, J.Q. Zhang, C.N. Cao, J. Electrochem. Soc. 150 (2003) A1399–A1404.
[33] Alexis Bienvenu Béléké, Eiji Higuchi, Hiroshi Inoue, Minoru Mizuhata, J. Power Sources 247 (2014) 572–578.
[34] J.H. Yao, Y.W. Li, Y.X. Li, Y.X. Zhu, H.B. Wang, J. Power Sources 224 (2013) 236–240.
[35] M. Hu, L.X. Lei, J.X. Chen, Y.M. Sun, Electrochim. Acta 56 (2011) 2862–2869.
[36] Q.D. Wu, S. Liu, L. Li, T.Y. Yan, X.P. Gao, J. Power Sources 186 (2009) 521–527.
[37] Q.D. Wu, X.P. Gao, G.R. Li, G.L. Pan, T.Y. Yan, H.Y. Zhu, J. Phys. Chem. C 111 (2007) 17082–17087.
[38] Alexis Bienvenu Bélékéa, Eiji Higuchi, Hiroshi Inoue, Minoru Mizuhata, J. Power Sources 225 (2013) 215–220.
[39] M. Hu, Z.Y. Yang, L.X. Lei, Y.M. Sun, J. Power Sources 196 (2011) 1569–1577.
[40] E.B. Shangguan, Z.R. Chang, H.W. Tang, X.Z. Yuan, H.J. Wang, Int. J. Hydrogen Energy 35 (2010) 9716–9724.
[41] E.B. Shangguan, Z.R. Chang, H.W. Tang, X.Z. Yuan, H.J. Wang, J. Power Sources 196 (2011) 7797–7805.
[42] L.X. Lei, M. Hu, X.R. Gao, Y.M. Sun, Electrochim. Acta 54 (2008) 671–676.
[43] A. Sugimoto, S. Ishida, K. Hanawa, J. Electrochem. Soc. 146 (1999) 1251–1255.
[44] D.N. Yang, R.M. Wang, M.S. He, J. Zhang, Z.F. Liu, J. Phys. Chem. 109 (2005) 7654–7658.
[45] S. Nathira Begum, V.S. Muralidharan, C. Ahmed Basha, Int. J. Hydrogen Energy 34 (2009) 1548–1555.
[46] Z.P. Xu, P.S. Braterman, J. Mater. Chem. 13 (2003) 268–273.
[47] Y.W. Li, J.H. Yao, Y.X. Zhu, Z.G. Zou, H.B. Wang, J. Power Sources 203 (2012) 177–183.
[48] Y.M. Wang, D.D. Zhao, Y.Q. Zhao, C.L. Xu, H.L. Li, RSC Adv. 2 (2012) 1074–1082.